Understanding the structure-property relationship in cortical bone to design a biomimetic composite

Flavia Libonati[1]*, Laura Vergani[1]

Politecnico di Milano, via G. La Masa 1, 20156 Milano, Italy

*Corresponding author, email address: flavia.libonati@polimi.it Phone: +39 02 2399 8667

Abstract: Bone is a hot topic for researchers, interested in understanding the structure-related properties of the tissue and the effect of aging, disease and therapies on that. A thorough understanding of the mechanical behavior of bone can be helpful to medical doctors to predict the fracture risk, but it can also serve as a guideline for engineers for the design of *de novo* biomimetic materials. In this paper, we show a complete characterization of cortical bone under static loading (i.e. tensile, compressive, three-point bending) and we carried out tests in presence of a crack to determine the fracture toughness. We performed all the tests on wet samples of cortical bone, taken from bovine femurs, by following the ASTM standards designed for metals and plastics. We also performed microscopic observations, to get an insight into the structure-property relationship. We noted that the mechanical response of bone is strictly related to the microstructure, which varies depending on the anatomical position. This confirms that the structure of bone is optimized, by nature, to withstand the different types of loads generally occurring in different body areas. The same approach could be followed for a proper biomimetic design of new composites.

Keywords: Cortical bone, characterization, microstructure, fracture, bioinspired composite.

Submitted to: Composite Structures

Nomenclature

a	Crack length
a_o	Initial crack length
E	Young modulus
σ_Y	Yield stress
σ_U	Ultimate strength
J, J_Q, J_{tot}	J-integral
J_c	Size-independent value of fracture thoughness
J_{el}	Elastic component of J-integral
J_{pl}	Plastic component of J-integral
A_{el}	Area of the elastic deformation underneath the load-displacement curve
A_{pl}	Area of the plastic deformation underneath the load-displacement curve
K_Q	Critical stress–intensity factor
K_{Ic}	Linear elastic fracture toughness (*i.e.* Critical value of K_I at fracture)
K_{Jc}	Equivalent fracture toughness
ν	Poisson's ratio
P	Load
P_Q	Load corresponding to the 5% deviation from linearity
P_{max}	Maximum load the sample is able to sustain
W	Specimen width
b_0, $W-a_0$	Uncracked ligament
B	Specimen thickness
$CMOD$	Crack mouth opening displacement

1. Introduction

Bone has gained an increasing attention among engineers, material scientists and biologists, thanks to its optimal combination of mechanical properties. It is generally considered the most important biological load-bearing material, providing support for many animal body structures, protecting internal organs, and along with muscles enabling movement.

Although bone has been studied for decades, it is still a hot topic for researchers. It is an extremely tough, lightweight, adaptive and multifunctional material. It is characterized by outstanding mechanical performance, in spite of its relatively poor constituents (*i.e.* collagen and hydroxyapatite). Its composite structure and complex hierarchical organization, spanning from the atomistic to the macroscale, make it a fascinating material, attracting many researchers from different fields. In particular, understanding the role of the multiscale organization is still a big challenge, and today, thanks to the recent innovative numerical and experimental techniques, it is possible to reach the nano- and sub-nanoscale. A representation of bone hierarchical structure, from the macroscale to the nanoscale, is given in Figure 1.

Quantitative assessment of the mechanical properties of bone, such as stiffness, strength and toughness, has become a crucial part of many biological and bioengineering studies [1-16]. Moreover, additional studies focus on the degradation of the bone mechanical properties due to aging, diseases and therapeutic treatments [17-24]. Indeed, biologists and medical doctors are mostly interested in understanding the effect of diseases and medical treatments on the tissue properties, whereas engineers are mainly interested in studying the mechanical properties and the structure-property relationship, with the purpose of mimicking these properties in the design of innovative smart materials.

Several studies on the mechanical characterization of bone have been carried out in the last decades, leading to a large amount of data available in the literature. Different techniques for bone characterization have been adopted at different length scales:

- At macroscale, conventional testing [2-4, 6, 7, 9, 10, 16, 25-29], but also ultrasounds [12, 30] have been used to characterize cortical and trabecular tissues, showing a clear anisotropy of bone;
- At microscale, Ascenzi and co-workers [31-35] have largely examined the anisotropic mechanical properties of single osteons by experimental measurements under different loading conditions (*i.e.* tension, compression, bending and torsion); other authors used micromechanical testing [7, 36, 37] and acoustic microscopy [15, 38, 39] to evaluate the elastic properties of bone at the microstructural level;
- At nanoscale, the most common technique used to characterize bone tissue is nanoindentation [13-15, 40, 41]. Moreover, novel less invasive methodologies for *in vivo* measuring fracture toughness on

small animals are of great clinical relevance, since they can be helpful in understanding the material properties of bone during preclinical testing for reducing fracture risks [42].

- At nano- to subnanoscale, numerical simulations - from atomistic to coarse grain - allow researchers to examine the small scale chemo-mechanical behavior, studying characteristic phenomena, which are difficult to be reached by experiments [43].

Besides the multiscale hierarchical structure, the presence and coexistence of many cracks and defects make this material intriguing. Indeed, in bone, there are many cracks due to the continuous loading, resulting from daily activities. What makes bone so attractive is the capacity of self-repairing. In particular, the combination of mechanical and metabolic activities allows small cracks to be removed before becoming sufficiently long to be dangerous. An extensive literature on the study of crack propagation and structure-induced toughening mechanisms exists. In particular, Ritchie *et al.* [3, 8, 44, 45] deeply analysed the fracture toughening mechanisms, such as osteon pullout, crack deflection, constrained microcracking, fiber bridging, that are characteristic of each hierarchical level. The combination of such toughnening mechanisms leads to an overall increase in bone toughness, especially if compared to the low toughness of its building blocks (*i.e.* collagen and hydroxyapatite).

Besides the hierarchy, bone properties are largely influenced by several factors, such as the type of tissue (*i.e.* cortical or trabecular), the age, the type of animal, but also the anatomical location (*i.e.* in the body). In fact, bone is a dynamic structure, able to adapt its architecture and properties to the different mechanical stimuli, characteristic of each anatomical position. The literature about mechanical testing of bone confirms a high variability of the mechanical properties. A literature review of the mechanical properties of cortical bone, determined by means of different experimental techniques, is given in Table 1.

There is a wide documentation regarding the experimental techniques for characterization of bone stiffness, strength, and for the determination of bone fracture toughness. However, there is not a universal procedure to be followed, for the determination of the structural properties. For this reason, in most studies, tests are generally carried out according to the reference standard procedures for metallic and plastic materials. Standards (*e.g.* ASTM) define the procedure to determine stiffness, strength and toughness in structural materials. However, the possibility of correctly applying them to biological materials is still under discussion.

Regarding the study of bone fracture resistance, several fracture mechanics test methods have been used to evaluate toughness, including: i) linear-elastic fracture mechanics (LEFM) fracture toughness (K_{Ic}) method [4, 21, 25, 46-48], ii) nonlinear fracture mechanics (NLFM) fracture toughness (J_c) method [2, 7, 49, 50], iii) determination of crack-resistance curves (R-curves) [2, 6, 7, 19, 51], and iv) other nonlinear methods [9, 52]. The choice of a specific method is a researcher's prerogative. However, according to the most recent papers, the procedures generally used for ductile materials seem to correctly apply to cortical bone. Regarding the

determination of fracture toughness, instead, the choice of LEFM method or NLFM one, also depends on the testing conditions (*e.g.* wet or dry), being bone extremely hygroscopic.

The core of this paper is to give a comprehensive characterization of cortical bone under quasi-static loading conditions and to validate our testing setup. The aim of this work is to get a thorough understanding of the mechanical behavior of cortical bone and the structure-property relationship that will serve as a guideline for an engineering design of *de novo* biomimetic materials. In a previous work [53], we showed a first example of an innovative bone-inspired design. In the following, we show the importance of the bone complex structure on the overall fracture behavior, and in particular, how the microstructural changes affect the mechanical performance, providing bone adaptation to different loading conditions, with the aim of reproducing the key microstructural features in the design of new biomimetic materials.

2. Materials and methods

In the following, we show: i) tensile tests, ii) compressive t., iii) three-point bending t., and iv) tests carried out in presence of a crack to determine the fracture toughness. These tests allowed us to determine the elastic modulus (E), yield stress (σ_Y), ultimate strength (σ_U), and fracture toughness (K_{Jc}). We performed all the tests on wet samples of bovine cortical bone, by following the ASTM standard generally adopted for metals and plastics. Furthermore, we performed several microscopic observations before testing, to verify whether bone microstructure was Haversian or plexiform. Additional microscopic observations were performed after testing, allowing us to get an insight into the structure-property relationship, by correlating the mechanical response and the failure mode with the microscopic structure.

2.1. Sample preparation

We obtained all the samples from three 18-months old bovine femurs, three days after slaughter. We cut the epiphyses, removed the marrow and cleaned the diaphysis. Then we cut samples by wet machining the cortical shell of the bone mid-shaft, by means of a low-speed saw and a milling machine. Being bone extremely hygroscopic and its properties strictly related to the water content, we paid attention to keep the material wet, during cutting, to prevent heating and changes in the mechanical properties. We stored all the samples in freezer, then in saline solution at 3 °C for 20 hours, then at room temperature for four hours until testing.

2.2. Experimental testing

To get a complete characterization of bone cortical tissue under static loading, we carried out experimental tests under different loading conditions: i) tensile, ii) compressive, iii) bending, and iv) in presence of a crack

to determine the fracture toughness. For all the tests, we used an MTS ALLIANCE RT/100 universal tensile testing machine, endowed with a 100 kN load cell and we adopted a data acquisition frequency of 20 Hz.

Moreover, to get a deeper understanding of its mechanical behavior, we performed microscopic observations, by means of an optical microscope (OM) and a scanning electron microscope (SEM).

Since there is not a reference standard for bone testing, we decided to perform tests according to the American standard defined for metals, as many other authors [51, 54]. A schematic representation of the types of samples and the loading conditions used in all the tests is given in Figure 2; highlighted also, the area of sample cutting.

2.2.1. Uniaxial tensile tests

We performed uniaxial tensile tests according to ASTM E8 [55], the standard designed by ASTM for tensile testing of metals, since bone is generally considered a ductile material. We used 11 dog bone specimens, 67 mm long with a circular cross section and a 3 mm nominal diameter (see Figure 2a). The length of the specimens corresponds to the longitudinal axis of the osteons. We performed tests in displacement control mode, with a crosshead speed of 1 mm/min, *i.e.* strain rate of $4 \cdot 10^{-4}$ s^{-1}, which corresponds to that experienced when walking [56]. To measure small local displacements we used an extensometer (MTS 632.26F-20) with an 8 mm gage length.

2.2.2. Uniaxial compressive tests

We performed uniaxial compressive tests by following ASTM E9 [57], the standard designed by ASTM for compressive testing of metallic materials but already adopted for bone compressive testing. There are not particular constraints regarding the geometry of the specimens, but it is recommended to use small heights to prevent buckling of the samples. In the literature, researchers generally use cubic or cylindrical specimens with height-to-diameter ratio equal to two. We used cylindrical specimens with 7 mm diameter and 14 mm height (see Figure 2b). We cut them by lathe machining, paying attention to have the upper and lower surfaces as parallel as possible. The height of the specimens corresponds to the longitudinal axis of the osteons. We polished the top and bottom sides to ensure parallel surfaces. In addition, in the testing setup to apply loads, we used plates with ball joints, able to compensate the imperfect parallelism between the top and bottom surfaces. We performed tests on 21 samples in displacement control mode, with a crosshead speed of 0.7 mm/min, corresponding to a strain rate of 10^{-3} s^{-1}, already adopted by other authors, and physiologically corresponding to walking [27, 56, 58]. We also performed some tests at different crosshead speed (*i.e.* 0.07 and 7 mm/min) to probe the effect of the velocity on the mechanical response. We loaded all the samples until compressive failure. To measure the small displacements we used an external deflectometer (MTS 632.06H-30).

2.2.3. Three-point bending tests

We examined the response of cortical bone under flexural loading by means of three-point bending tests. For this type of test, we followed the standard ASTM D790 [59], generally used for unreinforced plastics but also adopted for bone tissue [21, 37]. We cut rectangular specimens (50×8×4 mm), where the length of the specimens corresponds to the main axis of the osteons (see Figure 2c). In the testing setup we strictly followed the standard, ensuring the span length be four times the sample height. We carried out tests on four samples in displacement control mode, with a 0.5 mm/min crosshead speed.

2.2.4. Fracture toughness tests

To investigate the fracture behavior of cortical bone, we carried out fracture toughness tests, by following the American standard used to determine fracture toughness of metallic materials [60, 61], and generally adopted to perform the same measurements on bone [7, 21, 51, 62]. For this type of test we used two different sample geometries: compact tension samples, C(T), and single edge notched bending samples, SE(B).

To determine mode I fracture toughness, we cut six C(T) specimens with W = 25.4 mm and a through-thickness notch, extending over half of the specimen width (see Fig. 2e). The direction of the applied load is parallel to the main axis of the osteons, and the samples are subjected to a combined tensile-flexural loading. To get a sharp notch, allowing a local stress concentration, fatigue pre-cracking is generally required by the standard. However, bone is difficult to fatigue pre-crack because additional damage can be created, during crack propagation, and the crack path is normally not straight. Hence, to create a sharp notch, we used a razor blade and we measured the notch length (*i.e.* about 200 μm) by means of an optical microscope. We should underline that the dimensions of the C(T) samples do not properly follow the standard [60, 61]. Indeed, due to the limited depth of the cortical shell, the thickness of the specimens was 40 % less than the one suggested by the standard.

To determine the fracture toughness under a pure flexural loading, we carried out three-point bending fracture toughness tests on four SE(B) specimens with W = 12 mm and a through-thickness notch, extending over half of the specimen width (see Fig. 2d) and perpendicular to the longitudinal direction of the osteon. The specimen geometry followed the standard, being 70×12×6 mm. The span length, S, was chosen to be 4 times the width, W. We created the notch by means of a razor blade and we measured the extent of the notch (*i.e.* about 200 μm) by means of an optical microscope.

For both geometries, we cut the notch perpendicular to the longitudinal axis of the osteons, allowing us to study the transversal-fracture behavior of cortical bone. We carried out all fracture toughness tests in displacement control mode and we applied the load through pin loading clevises, choosing a 0.1 mm/min

crosshead speed. To measure the crack mouth opening displacement (CMOD) we used an MTS 632.02F-20 clip-on gage.

First we calculated the critical stress-intensity factor, K_Q, using Eq. (1) for C(T) and Eq. (2) for SE(B) samples:

$$K_Q = \frac{P_Q}{B\sqrt{W}} \cdot f\left(\frac{a}{W}\right) \quad (1)$$

$$K_Q = \frac{P_Q \cdot S}{B \cdot W^{3/2}} \cdot f\left(\frac{a}{W}\right) \quad (2)$$

Where *f(a/W)* is the corresponding shape function as defined in the standard [60]. The ASTM E399 [60] allows the determination of K_{Ic} values, upon agreement of small-scale yielding, as given in Eq. (3):

$$P_{max}/P_Q \leq 1.1 \quad (3)$$

and plain strain conditions (*i.e.* the plastic zone must be small enough compared to the notch length, a, the uncracked ligament, W-a, and the thickness, B), as shown in Eq. (4):

$$B, a, (W-a) > 2.5\left(\frac{K_Q}{\sigma_Y}\right)^2 \quad (4)$$

Meeting the thickness and ligament size and the linear-elastic conditions cannot be ensured in advance. Hence, after testing we verified whether those conditions were satisfied. K_{Ic} is a single point value of fracture toughness and represents the resistance to crack initiation, whereas the J integral, evaluated through a tearing resistance curve (*i.e.* R-curve) represents the resistance to crack growth. According to ASTM E399 [60], both the conditions expressed by Eq. (3)-(4) must be satisfied. However, due to the non-negligible inelastic deformations, occurring during testing, and probably due to local microdamage (*e.g.* microcracking) and plasticity or viscoelasticity, Eq. (3) was not satisfied. Hence, we calculated the fracture toughness at instability using the J-integral, that estimates the total energy (*i.e.* both elastic and plastic) spent before fracture [61]. We calculated J_{tot} or J_Q at the final point of instability, as follows in Eq. (5):

$$J_{tot} = J_{el} + J_{pl} = \frac{K^2 \cdot (1-\nu^2)}{E} + \frac{\eta_{pl} \cdot A_{pl}}{B \cdot b_0} \quad (5)$$

To qualify J_Q as J_C, a size-independent value of fracture toughness, we verified that the thickness and ligament size conditions were met, as from Eq.(6):

$$B, b_0 > 100 J_Q/\sigma_Y \quad (6)$$

Also, from J_c we calculated the equivalent fracture toughness, K_{Jc}, as defined in Eq. (7):

$$K_{Jc} = \sqrt{J_c \cdot E'} \quad (7)$$

Where E', the elastic constrained modulus is defined as $E' = E/(1-\nu^2)$. The elastic modulus, E, was determined from the tensile tests, whereas for Poisson ratio, ν, we considered a value equal to 0.4, as average from the literature values.

We should underline that the determined K_Q can only be estimated values and not K_{Ic} ASTM standard values [60, 61]. Also, for the case of C(T) specimens, the J_c values are not accurate. Indeed, being the samples designed according to ASTM E399 [60], we measured the CMOD and not the load-line displacement as required by [61].

2.3. Microscopic analyses

To observe the microstructure of cortical bone before testing, we used an optical microscope (LEITZ WETZLAR GmbH type 307-148-002). We accurately polished the surfaces of untested samples by means of silicon carbide papers of increasing grit numbers (600, 800, 1200, 2500), then sonicated in distilled water. We performed a final polishing, by means of diamond abrasive cloth and we performed again an ultrasonic cleaning to remove any residual particle adhering to the polished surfaces.

We also used an SEM Evo 50 EP Zeiss, Oxford Instruments, to observe the fracture surfaces after testing. We previously dehydrated the samples and then gold sputtered the surfaces to make them conductive. We observed the samples in high vacuum conditions, by means of secondary electrons.

3. Results

The outcome of the experimental tests showed a good agreement with the literature [49, 51], confirming the validity of our testing setup. In addition, the experimental results revealed a good repeatability, although in some cases we noticed a high scattering, probably owing to the difference in the sample microstructure. This confirms the literature trend. Indeed, there is a large amount of literature data on the characterization of cortical bone tissue. However, these data show a high variability, being bone properties influenced by several factors such as age, microstructure, and anatomical area. The results obtained from the experimental tests are summarized in Table 2 and discussed, in detail, in the following sessions. Figure 3 shows the failure mode of all samples, subjected to different types of tests.

3.1.1. Uniaxial tensile tests

The results of the tensile tests showed a ductile-to-fragile behavior of bone, as shown in Figure 4. Indeed, by carefully looking at the stress-strain curves, resulted from the tensile tests, it is possible to distinguish two types of mechanical behavior: a linear elastic behavior (Figure 4c) and an elastic-plastic one (Figure 4d). We noticed that the samples showing a linear elastic behavior were those, cut from the anterior region of the

diaphysis (*i.e.* region 1 indicated in Figure 4b), whereas the samples characterized by an elastic-plastic behavior were those, cut from the lateral-to-posterior region (*i.e.* region 2-3 indicated in Figure 4b). This trend confirms a strong correlation between the mechanical behavior and the anatomical location and it would merit further investigation. This difference in the mechanical behavior correspond to a different failure mode. Although all the specimens showed a failure surface transversal to the applied load (see Figure 3a), by analyzing the fracture surfaces it is possible to distinguish a fragile failure mode, characterized by a more fibrous surface, from a more ductile one, with a rough and jagged surface.

3.1.2. Uniaxial compressive tests

The results of compressive tests are comparable with those found by Novitskaya et al. [27, 58]. However, those results showed a certain scattering. We also investigated the effect of the strain rate, by carrying out additional tests adopting a one order of magnitude higher and lower strain rate. However, we could not prove a clear effect of the strain rate on the overall mechanical response of the bone tissue, under compressive loading. Although the scattering of the results, as shown in Figure 5, the failure mode is similar for all the samples and occurred on a plane oriented at 45° with respect to the loading direction, as shown in Figure 3b. The fracture surfaces are typical of those of ductile materials, and looked, by bare eyes, very rough and jagged.

By further analyzing the stress-strain curves, we found a correlation between the different mechanical behavior and the anatomical location of each sample, proving again a strong relationship between the microstructure, the anatomical position and the mechanical performance. In particular, the results of compressive tests show how the mechanical properties changes not only through the cross section, but also along the length of the femur. Here a systematic investigation on the effect of anatomical location on the mechanical compressive response is needed. In particular, we expect a strong correlation between the anatomical position, the microstructure and the mechanical response.

The changes in the mechanical response are due to a change in the microstructure. Indeed, as previously shown in [63], bone microstructure varies in the cross section and along the femur length, and this represents an adaptation to local mechanical stimuli. In particular, the Haversian structure is thought to be an adaptation to high compressive stresses. Hence, the remodeling process, is very likely to be steered by compressive stresses. This was another confirmation that bone is designed, by nature, to give an optimal response to the mechanical stimuli, which is subjected to.

3.1.3. Three-point bending tests

The results of three point bending tests were repeatable, showing a flexural stiffness of 11.5 ± 0.6 GPa and a bending strength of 223.4 ± 9.5 MPa, as shown in Table 2 and in Figure 6. The cortical bone tissue showed a

good mechanical behavior under flexural loading. Indeed, this type of loading condition is very common in human and bovine femur, leading to a typical stress distribution, characterized by both tensile and compressive stresses. The areas, mainly characterized by compressive stresses, are generally more involved in the remodeling process, hence characterized by a clear Haversian secondary structure (*i.e.* with high density of secondary osteons). In all the samples failure occurred transversely to the main osteon direction, and it was characterized by a zigzag crack path and rough ductile-like fracture surface.

3.1.4. Fracture toughness tests

The results of the fracture toughness tests were repeatable. After post processing the results, we could confirm that all the fracture toughness tests did not meet the linear-elastic condition as required by the standard [60]. Indeed, during the tests we observed a rather plastic behavior, which required the adoption of nonlinear fracture mechanics.

We initially determined fracture toughness as K_Q = 4.4 ± 0.8 MPa√m for SE(B) specimens and K_Q = 5.4 ± 0.8 MPa√m for C(T) specimens. Then, we determined the *J*-integral as defined in Eq. (5), according to ASTM E1820 [61], and the equivalent fracture toughness, K_{Jc} as defined in Eq. (7). The latter is a measurement of fracture toughness at crack initiation. The obtained values are listed in Table 2: for SE(B) specimens we obtained J = 4.9 ± 1.7 kJ/m^2, whereas for the C(T) ones J = 4.4 ± 1.7 kJ/m^2. These correspond to K_{Jc} = 10.6 ± 1.7 MPa√m and K_{Jc} = 10.0 ± 1.8 MPa√m, for SE(B) and for C(T) specimens, respectively. These results are consistent with the literature data [49, 51, 64] related to experimental testing carried out on bovine cortical bone. By analyzing the *J*-integral data, we realized that the contribution of plastic deformation, measured as the J_{pl}/J_{tot} ratio, is consistent and corresponds to 60%. This endorses the use of the NLFM method for future testing. Then, by comparing the failure stress of SE(B) specimens to the failure stress of specimens subjected to three point bending tests, we noticed only 13% reduction, meaning that the presence of a crack slightly affected the fracture behavior.

In all the tests, we investigated the transversal fracture toughness, where transversal refers to a direction orthogonal to the osteon main axis. As expected, the fracture mode is different from traditional materials such as steel. For SE(B) specimens, the crack does not show a straight path, but many deviations, and the fracture surface is generally rough, sign of absorption of a large amount of energy before fracture. For C(T) specimens instead, the crack generally shows a 90° deviation and tends to propagate parallel to the osteon main axis, probably along the weak osteon-osteon interface, and leading to longitudinal splitting. The difference in crack propagation between SE(B) and C(T) corresponds to a difference in the fracture surfaces.

3.1.5. Microscopic analyses

Figure 7 shows microscopic images, by OM, performed to probe whether the microstructure was Haversian or plexiform, and to detect the presence of intrinsic defects and manufacturing-induced microdamages. Most of the specimens showed a secondary or Haversian microstructure (see Figure 7a), whereas other samples showed a primary, or plexiform structure (see Figure 7b). We also noticed that in the femur cross section there is a transition, from an osteonal region, corresponding to the inner part of the femur, close to the marrow, to a more plexiform region, corresponding to the outer part, close to the outer cortex. The difference in the microstructure unravels the riddle of different mechanical responses shown by different samples. The microscopic images also show the presence of many defects, such as porosities, delamination between different circumferential lamellae, and cracks, tens of microns long. The cracks, probably induced by sample manufacturing, never show a linear path. Instead, they have a clear interaction with the microstructure proving a crucial role, played by osteons, and probably by the cement lines. We noticed that the osteons are sites of cracks: indeed, microcracks originate from osteons, from porosities and canals, which act then as stress concentration zones.

Figure 8 shows the SEM microscopic images of the fracture surfaces. A first analysis, by bare eyes, allowed us to see the different failure mode that characterized the SE(B) and C(T) samples. The former showed a rougher surface, characteristic of a ductile behavior, whereas the latter showed a smoother surface. Indeed, in C(T) samples the final rupture occurred by longitudinal splitting, while in SE(B) samples the final breakage occurred transversally. By observing the microscopic image in Figure 8a, relative to the fracture surface of an SE(B) sample, it is possible to see a very rough surface with consistent inelastic deformations, characteristic of a non-brittle material. A more in depth analysis of the image allows one to identify the classic toughening mechanisms of crack deviation, largely discussed in the literature and predicted by our previous numerical study [65], and osteon pullout. In Figure 8b instead, we show the fracture surface of a C(T) sample. The surface is less rough than that shown in Figure 8a, due to a different failure mode. Indeed, in this case the crack showed a 90° deflection and the sample failed by longitudinal splitting. The images taken with an SEM confirmed the difference in the failure mode of SE(B) and C(T) samples. This difference might be due to the slightly different loading conditions. In fact, SE(B) are subjected to pure bending; C(T) instead are subjected to a combination bending and tensile loads, though the tensile stress acting at the crack tip is considerably lower than the bending one. This aspect is very interesting and it may need further investigation.

4. Discussion

The above presented results showed a good comparison with the literature [27, 49, 51, 64], allowing us to validate the adopted testing setup and propose it for further studies.

From the outcome of the tests, it is possible to distinguish a brittle-to-ductile behavior. The different behavior is mainly due to a different microstructure, which represents an adaptation of bone to different mechanical loads, characteristic of each anatomical region. Indeed, by observing the stress-strain curves of each sample, we found a correlation between the mechanical behavior and the anatomical location of the corresponding sample, proving a strong relationship between the anatomical area and the mechanical performance. In addition, the microscopic images showed different microstructures (from Haversian to plexiform) found in the cortical bone samples, taken from the same femur. The difference in the microstructure unravels the question of the different mechanical responses shown by different samples. This is an experimental proof of the adaptation of bone microstructure to the local mechanical stresses, already proposed by other authors [63].

Regarding the determination of fracture toughness, here we mainly focused on ductile initial cracking and we measured the fracture toughness as resistance to crack initiation. Nevertheless, as broadly shown in previous studies, the fracture toughness, intended as resistance to crack growth, increases with crack propagation, in contrast to brittle materials, where toughness remains constant regardless the crack extent [5, 6, 51]. This makes bone more resistant to crack propagation than crack initiation. This aspect requires a further investigation, by using the NLFM method for the determination of the fracture toughness and the determination of crack-resistance curve (R-curve).

By observing the fracture behavior, we noticed a dependence on water content. In particular, some specimens, which were removed from solution not immediately before testing, experienced a more brittle behavior. The mechanical response depends on water content. Indeed, bone is a highly hygroscopic material, whose water and protein content affects the ability of deforming and dissipating energy under mechanical loading, leading to a more ductile material. The reasons of this behavior have to be sought at smaller length scales, where H-bonds act as “sacrificial” bonds, increasing the deformation ability and the energy to failure [66]. We did not perform the tests in water, but we paid attention to keep samples in saline solution until testing. For this reason, our results are comparable with those of hydrated samples found in [49, 64].

Microscopic images of untested bone samples were useful to observe the microstructure and the presence of intrinsic defects and manufacturing induced microdamages. The observation of the fracture surfaces of the samples, previously subjected to fracture toughness tests, allowed us to get a better understating of the failure process and to detect the principal toughening mechanisms, to be mimicked in de novo composite materials. The microscopic observations confirmed that the main toughening mechanisms involved in the fracture process are crack deviation, largely discussed in the literature and also predicted by our previous numerical study [65], longitudinal splitting and osteon pull-out. These mechanisms, which increase the dissipation energy and the overall toughness, have shown to be strictly related to the presence of the

osteons. This demonstrate the key role played by the microstructure, and by its characteristic feature (i.e. the osteon) in activating the principal toughening mechanisms, affecting the fracture behavior of the bone.

5. Final Remarks

In this paper, we provide a comprehensive characterization of cortical bone with the aim of getting an insight into the structure-property relationship. Indeed, understanding how the microstructure of cortical bone affects the mechanical behavior is crucial for the design of a bone-inspired composite.

In a nutshell, our study shows that:

- Bone behavior is strictly dependent upon the anatomical location (*i.e.* sample cutting area). Samples taken from different regions showed different microstructural patterns and different behaviors, failing in a brittle-to-ductile fashion. This is particularly evident from the tensile results.
- Bone mechanical response is strictly correlated to the applied load. A small difference in the loading conditions can affect the overall fracture response, as resulted from fracture toughness tests. The different failure mode of SE(B) and C(T) sample is interesting and worthy of additional study.
- The hierarchical structure activates different toughening mechanisms occurring at different length scales, leading to a larger dissipation of energy before fracture. Here we mainly observed the microstructure-related toughening mechanisms, such as formation of microcracks, crack deviation and twisting and longitudinal splitting.
- Linear elastic fracture mechanics, largely used by several authors to determine the fracture toughness of bone, has shown not to be the most appropriate method to describe the bone fracture behavior. Indeed, in wet conditions, the plastic contribution is non-negligible and the bone tissue has shown to absorb large amount of energy in inelastic deformation before fracture. It is important to stress that inelastic deformations include plasticity but also different types of structure-related dissipation mechanisms, characteristic of the bone tissue (e.g. formation of microcracks, crack deviation).

We show the possibility of adapting testing benchmarks, generally adopted for structural materials, to perform experimental measurements of bone mechanical properties. Nevertheless, to improve the testing setup, we suggest:

I. To directly follow the ASTM E1820 [61], using nonlinear elastic *J*-integral measurements to include the role of plastic deformation in the determination of the fracture toughness. Moreover, a single value toughness test is not ideal for bone material, since the toughness increases with crack growth and is best captured through a crack-growth resistance curve (R-curve).

II. To provide the specimens for fracture toughness tests with side grooves that help controlling the crack propagation. Indeed, in bone, the crack can deviate from the main direction, causing large variation in the experimental results.

In this study, we raised important questions: in particular, the unusual brittle-to-ductile behavior under tensile loading, and the different failure modes observed during fracture toughness tests. These points would certainly need further research with the aim of finding a quantitative correlation between the anatomical position, the local microstructure and the mechanical response.

We showed the importance of the microstructural organization in the fracture behavior, proving that a thorough understanding of the mechanical behavior of bone and the correlation with its structure can serve as an engineering guide for the design of *de novo* biomimetic materials. Our goal is to replicate the Haversian structure in new biomimetic composite materials, starting from the microstructural key features, such as osteons. We aim to improve our first biomimetic designed presented in [53], where we demonstrated the crucial role played by the osteons in affecting the crack path. The outcome of this study will be helpful for improving the previous design, and provide the basis for the design of new bio-inspired composites.

Acknowledgements

We acknowledge the technicians of the laboratories of Mechanical Engineering Department and Biomedical Engineering Department, for the support given for sample cutting and for the testing setup.

References

[1] Katz JL. Mechanical properties of bone. In: ASME, editor.: American Society of Mechanical Engineers; 1981, p. 171-184.
[2] Koester KJ, Ager JW, Ritchie RO. The true toughness of human cortical bone measured with realistically short cracks. Nature Materials 2008;7: 672-677.
[3] Launey ME, Buehler MJ, Ritchie RO. On the Mechanistic Origins of Toughness in Bone. Annual Review of Materials Research 2010;40: 25-53.
[4] Nalla RK, Kinney JH, Ritchie RO. Mechanistic fracture criteria for the failure of human cortical bone. Nature Materials 2003;2: 164-168.
[5] Nalla RK, Stölken JS, Kinney JH, Ritchie RO. Fracture in human cortical bone: local fracture criteria and toughening mechanisms. Journal of Biomechanics 2005;38: 1517-1525.
[6] Nalla RK, Kruzic JJ, Kinney JH, Ritchie RO. Mechanistic aspects of fracture and R-curve behavior in human cortical bone. Biomaterials 2005;26: 217-231.
[7] Ritchie RO, Koester KJ, Ionova S, Yao W, Lane NE, Ager JW, 3rd. Measurement of the toughness of bone: a tutorial with special reference to small animal studies. In: Bone. United States; 2008, p. 798-812.
[8] Ritchie RO, Buehler MJ, Hansma P. Plasticity and toughness in bone. Physics Today 2009;62: 41-47.
[9] Yang QD, Cox BN, Nalla RK, Ritchie RO. Re-evaluating the toughness of human cortical bone. Bone 2006;38: 878-887.

[10] Zimmermann EA, Launey ME, Barth HD, Ritchie RO. Mixed-mode fracture of human cortical bone. Biomaterials 2009;30: 5877-5884.
[11] McNamara LM. Bone as a Material: Elsevier Science; 2011.
[12] Ashman RB, Rho JY. Elastic modulus of trabecular bone material. Journal of Biomechanics 1988;21: 177-181.
[13] Rho J-Y, Tsui TY, Pharr GM. Elastic properties of human cortical and trabecular lamellar bone measured by nanoindentation. Biomaterials 1997;18: 1325-1330.
[14] Rho J-Y, Roy ME, Tsui TY, Pharr GM. Elastic properties of microstructural components of human bone tissue as measured by nanoindentation. Journal of Biomedical Materials Research 1999;45: 48-54.
[15] Turner CH, Rho J, Takano Y, Tsui TY, Pharr GM. The elastic properties of trabecular and cortical bone tissues are similar: results from two microscopic measurement techniques. Journal of Biomechanics 1999;32: 437-441.
[16] Rho J-Y, Kuhn-Spearing L, Zioupos P. Mechanical properties and the hierarchical structure of bone. Medical Engineering & Physics 1998;20: 92-102.
[17] Busse B, Bale HA, Zimmermann EA, Panganiban B, Barth HD, Carriero A, Vettorazzi E, Zustin J, Hahn M, Ager JW, Püschel K, Amling M, Ritchie RO. Vitamin D Deficiency Induces Early Signs of Aging in Human Bone, Increasing the Risk of Fracture. Science Translational Medicine 2013;5: 193ra88.
[18] McBride JDJ, Shapiro JR, Dunn MG. Bone Geometry and Strength Measurements in Aging Mice with the oim Mutation. Calcified tissue international 1998;62: 172-176.
[19] Nalla RK, Kruzic JJ, Kinney JH, Ritchie RO. Effect of aging on the toughness of human cortical bone: evaluation by R-curves. Bone 2004;35: 1240-1246.
[20] Ritchie RO, Nalla RK, Kruzic JJ, Ager JW, Balooch G, Kinney JH. Fracture and Ageing in Bone: Toughness and Structural Characterization. Strain 2006;42: 225-232.
[21] Zioupos P, Currey JD. Changes in the Stiffness, Strength, and Toughness of Human Cortical Bone With Age. Bone 1998;22: 57-66.
[22] Chang S-W, Shefelbine Sandra J, Buehler Markus J. Structural and Mechanical Differences between Collagen Homo- and Heterotrimers: Relevance for the Molecular Origin of Brittle Bone Disease. Biophysical Journal 2012;102: 640-648.
[23] Camacho NP, Hou L, Toledano TR, Ilg WA, Brayton CF, Raggio CL, Root L, Boskey AL. The Material Basis for Reduced Mechanical Properties in oim Mice Bones. Journal of Bone and Mineral Research 1999;14: 264-272.
[24] Wang X, Shen X, Li X, Mauli Agrawal C. Age-related changes in the collagen network and toughness of bone. Bone 2002;31: 1-7.
[25] Bonfield W. Advances in the fracture mechanics of cortical bone. Journal of Biomechanics 1987;20: 1071-1081.
[26] Turner CH, Burr DB. Basic biomechanical measurements of bone: A tutorial. Bone 1993;14: 595-608.
[27] Novitskaya E, Chen P-Y, Lee S, Castro-Ceseña A, Hirata G, Lubarda VA, McKittrick J. Anisotropy in the compressive mechanical properties of bovine cortical bone and the mineral and protein constituents. Acta Biomaterialia 2011;7: 3170-3177.
[28] Thurner PJ, Erickson B, Jungmann R, Schriock Z, Weaver JC, Fantner GE, Schitter G, Morse DE, Hansma PK. High-speed photography of compressed human trabecular bone correlates whitening to microscopic damage. Engineering Fracture Mechanics 2007;74: 1928-1941.
[29] Munch E, Launey ME, Alsem DH, Saiz E, Tomsia AP, Ritchie RO. Tough, bio-inspired hybrid materials. Science 2008;322: 1516.
[30] Rho JY, Ashman RB, Turner CH. Young's modulus of trabecular and cortical bone material: Ultrasonic and microtensile measurements. Journal of Biomechanics 1993;26: 111-119.
[31] Ascenzi A, Bonucci E. The tensile properties of single osteons. The Anatomical Record 1967;158: 375-386.
[32] Ascenzi A, Bonucci E. The compressive properties of single osteons as a problem of molecular biology. Calcified Tissue Research 1968;2: 44-44a.
[33] Ascenzi A, Bonucci E. Mechanical similarities between alternate osteons and cross-ply laminates. Journal of Biomechanics 1976;9: 65-71.

[34] Ascenzi A, Baschieri P, Benvenuti A. The bending properties of single osteons. Journal of Biomechanics 1990;23: 763-771.
[35] Ascenzi A, Baschieri P, Benvenuti A. The torsional properties of single selected osteons. Journal of Biomechanics 1994;27: 875-884.
[36] Choi K, Kuhn JL, Ciarelli MJ, Goldstein SA. The elastic moduli of human subchondral, trabecular, and cortical bone tissue and the size-dependency of cortical bone modulus. Journal of Biomechanics 1990;23: 1103-1113.
[37] Albert CI, Jameson J, Harris G. Design and validation of bending test method for characterization of miniature pediatric cortical bone specimens. Proc Inst Mech Eng H 2013;227: 105-13.
[38] Hasegawa K, Turner CH, Recker RR, Wu E, Burr DB. Elastic properties of osteoporotic bone measured by scanning acoustic microscopy. Bone 1995;16: 85-90.
[39] Katz JL, Meunier A. Scanning acoustic microscope studies of the elastic properties of osteons and osteon lamellae. J Biomech Eng 1993;115: 543-8.
[40] Saber-Samandari S, Gross KA. Micromechanical properties of single crystal hydroxyapatite by nanoindentation. Acta Biomaterialia 2009;5: 2206-2212.
[41] Zysset PK, Edward Guo X, Edward Hoffler C, Moore KE, Goldstein SA. Elastic modulus and hardness of cortical and trabecular bone lamellae measured by nanoindentation in the human femur. Journal of Biomechanics 1999;32: 1005-1012.
[42] Carriero A, Bruse JL, Oldknow KJ, Millán JL, Farquharson C, Shefelbine SJ. Reference point indentation is not indicative of whole mouse bone measures of stress intensity fracture toughness. Bone 2014;69: 174-179.
[43] Arun KN, Flavia L, Zhao Q, Leon SD, Markus JB. Mechanical and interface properties of biominerals: Atomistic to coarse grained modeling. In: DiMasi E, Gower LB, editors. Biomineralization Sourcebook: Characterization of biomineral and biomimetic materials: CRC Press; 2014, p. 337-351.
[44] Ritchie RO, Kruzic JJ, Muhlstein CL, Nalla RK, Stach EA. Characteristic dimensions and the micro-mechanisms of fracture and fatigue in `nano' and `bio' materials. International Journal of Fracture 2004;128: 1-15.
[45] Espinosa HD, Rim JE, Barthelat F, Buehler MJ. Merger of structure and material in nacre and bone – Perspectives on de novo biomimetic materials. Progress in Materials Science 2009;54: 1059-1100.
[46] Wright TM, Hayes WC. Fracture mechanics parameters for compact bone—Effects of density and specimen thickness. Journal of Biomechanics 1977;10: 419-430.
[47] Norman TL, Nivargikar SV, Burr DB. Resistance to crack growth in human cortical bone is greater in shear than in tension. Journal of Biomechanics 1996;29: 1023-1031.
[48] Phelps JB, Hubbard GB, Wang X, Agrawal CM. Microstructural heterogeneity and the fracture toughness of bone. In: J Biomed Mater Res. United States; 2000, p. 735-41.
[49] Yan J, Mecholsky Jr JJ, Clifton KB. How tough is bone? Application of elastic–plastic fracture mechanics to bone. Bone 2007;40: 479-484.
[50] Yan J, Taskonak B, Platt JA, Mecholsky Jr JJ. Evaluation of fracture toughness of human dentin using elastic–plastic fracture mechanics. Journal of Biomechanics 2008;41: 1253-1259.
[51] Vashishth D, Behiri JC, Bonfield W. Crack growth resistance in cortical bone: Concept of microcrack toughening. Journal of Biomechanics 1997;30: 763-769.
[52] Yang QD, Cox BN, Nalla RK, Ritchie RO. Fracture length scales in human cortical bone: The necessity of nonlinear fracture models. Biomaterials 2006;27: 2095-2113.
[53] Libonati F, Colombo C, Vergani L. Design and characterization of a biomimetic composite inspired to human bone. Fatigue & Fracture of Engineering Materials & Structures 2014;37: 772-781.
[54] Yamaguchi H, Kikugawa H, Asaka T, Kasuya H, Kuninori M. Determination of cortical bone strain distribution using image correlation techniques and fracture toughness. Nippon Kinzoku Gakkaishi/Journal of the Japan Institute of Metals 2010;74: 214-220.
[55] ASTM. E8/E8M - Standard Test Method for Tension Testing of Metallic Materials. In: ASTM, editor.; 2013.
[56] Zimmermann EA, Gludovatz B, Schaible E, Busse B, Ritchie RO. Fracture resistance of human cortical bone across multiple length-scales at physiological strain rates. Biomaterials 2014;35: 5472-81.

[57] ASTM. E9 - Standard Test Methods of Compression Testing of Metallic Materials at Room Temperature. 2009.
[58] Li S, Demirci E, Silberschmidt VV. Variability and anisotropy of mechanical behavior of cortical bone in tension and compression. Journal of the Mechanical Behavior of Biomedical Materials 2013;21: 109-120.
[59] ASTM. D790 - Standard Test Methods for Flexural Properties of Unreinforced and Reinforced Plastics and Electrical Insulating Materials. In: ASTM; 2010.
[60] ASTM. E399 - Standard Test Method for Linear-Elastic Plane-Strain Fracture Toughness K_{Ic} of Metallic Materials In; 2012.
[61] ASTM. E1820 - Standard Test Method for Measurement of Fracture Toughness. In; 2013.
[62] Li S, Abdel-Wahab A, Silberschmidt VV. Analysis of fracture processes in cortical bone tissue. Engineering Fracture Mechanics 2013;110: 448-458.
[63] Mayya A, Banerjee A, Rajesh R. Mammalian cortical bone in tension is non-Haversian. Sci. Rep. 2013;3.
[64] Yan J, Daga A, Kumar R, Mecholsky JJ. Fracture toughness and work of fracture of hydrated, dehydrated, and ashed bovine bone. Journal of Biomechanics 2008;41: 1929-1936.
[65] Vergani L, Colombo C, Libonati F. Crack Propagation in Cortical Bone: A Numerical Study. Procedia Materials Science 2014;3: 1524-1529.
[66] Libonati F, Nair AK, Vergani L, Buehler MJ. Mechanics of collagen–hydroxyapatite model nanocomposites. Mechanics Research Communications 2014;58: 17-23.

List of Tables.

Table 1 - Literature review of the mechanical properties of human and bovine cortical bone tissues, experimentally determined through different techniques.

Authors	Type of bone	E [GPa]	J_c [N/m]	K_c [MPa$\sqrt{m}$]	K_{Jlc} [MPa$\sqrt{m}$]	Test method
Rho *et al.* [13]	Cortical (human tibia)	22.5 ± 1.3 (osteon tissue) 25.8 ± 0.7 (interstitial lamellae)	-	-	-	Nanoindentation
Thurner *et al.* [15]	Cortical (human femur)	20.55±0.21 (longitudinal) 23.45±0.21 (longitudinal)	-	-	-	Acoustic measurement Nanoindentation
Rho *et al*. [30]	Cortical (human)	20.7 ± 1.9 * 18.6 ± 3.5 **	-	-	-	*Ultrasonic technique **Microtensile testing
Zysset *et al.* [41]	Cortical (human femur)	20.1±5.4	-	-	-	Nanoindentation
Vashishth *et al.* [51]	Cortical (bovine femur)	-	-	3.9-7.2	-	Fracture toughness tests on C(T) samples
Yan *et al.* [49]	Cortical (bovine femur)	17.5 (transverse-fractured) 12.1 (longitudinal-fractured)	6.6 ± 0.8 2.3 ± 0.3	5.1 ± 0.5 2.6 ± 0.3	10.5 ± 0.5 6.2 ± 0.3	Fracture toughness tests on SE(B) (with grooves)
Koester *et al.* [2]	Cortical (human humerus)	-	-	-	25 (crack length < 500 μm) 5 (crack length 7000 μm)	Fracture toughness tests on SE(B) and C(T) samples
Zimmermann *et al.* [56]	Cortical (human femur)	15.70 ± 3.5 (young) 15.85 ± 3.3 (aged)	-	-	11-14 (stress intensity rate 0.01 MPa$\sqrt{m}\cdot s^{-1}$	Fracture toughness tests on SE(B) samples

Table 2 - Experimental results of the mechanical characterization performed on cortical bovine bone samples. For the determination of K_{Jc} we used the value of E', calculated from the Young modulus, E, experimentally determined by means of tensile tests.

	Tensile test	Compression test	Flexural test	Fracture Toughness test SE(B)	Fracture Toughness test C(T)
***E* [GPa]**	19.6 ± 4.5	12.4 ± 3.2	11.5 ± 0.6	-	-
σ_y [MPa]	105.3 ± 26.1	145.5 ± 36.8	-	-	-
σ_U [MPa]	111.3 ± 27.4	149.1 ± 37.2	223.4 ± 9.5	-	-
K_Q [MPa√m] (E399) [60]	-	-	-	4.4 ± 0.8	5.4 ± 0.8
J_{tot} [KJ/m^2] (ASTM E1820) [61]	-	-	-	4.9 ± 1.7	4.4 ± 1.7[1]
K_{Jc} [MPa√m] (ASTM E1820) [61]	-	-	-	10.6 ± 1.7	10.0 ± 1.8[1]

[1]The values of J_c and K_{Jc} are only estimates, since the C(T) samples are designed according to ASTM E399 [60], hence we did not measure the load-line displacement as required by [61].

List of Figures.

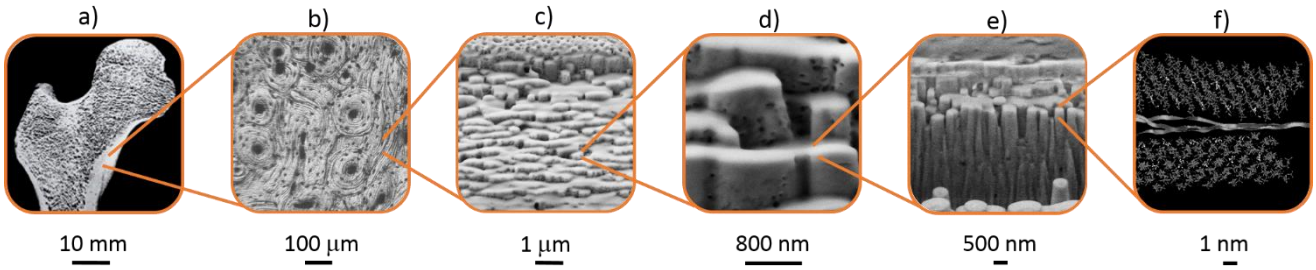

Figure 1 – Bone multiscale hierarchical structure: a) Bone structure at macroscale, where it is possible to distinguish the cortical or hard tissue and the trabecular or spongy one. b) Microstructure of cortical bone, also known as Haversian structure; it is possible to recognize the characteristic cylindrical feature (*i.e.* osteon). c) Circumferential lamellae. d) Collagen fiber bundles. e) Collagen mineralized fibrils. f) Single tropocollagen molecule surrounded by Hydroxyapatite nanocrystals. The picture shown in b) was taken by means of an optical microscope, pictures represented in c)-d)-e) were taken by means of an SEM after an FIB (focus ion beam) cutting, and figure f) is from atomistic simulations of collagen-hydroxyapatite system.

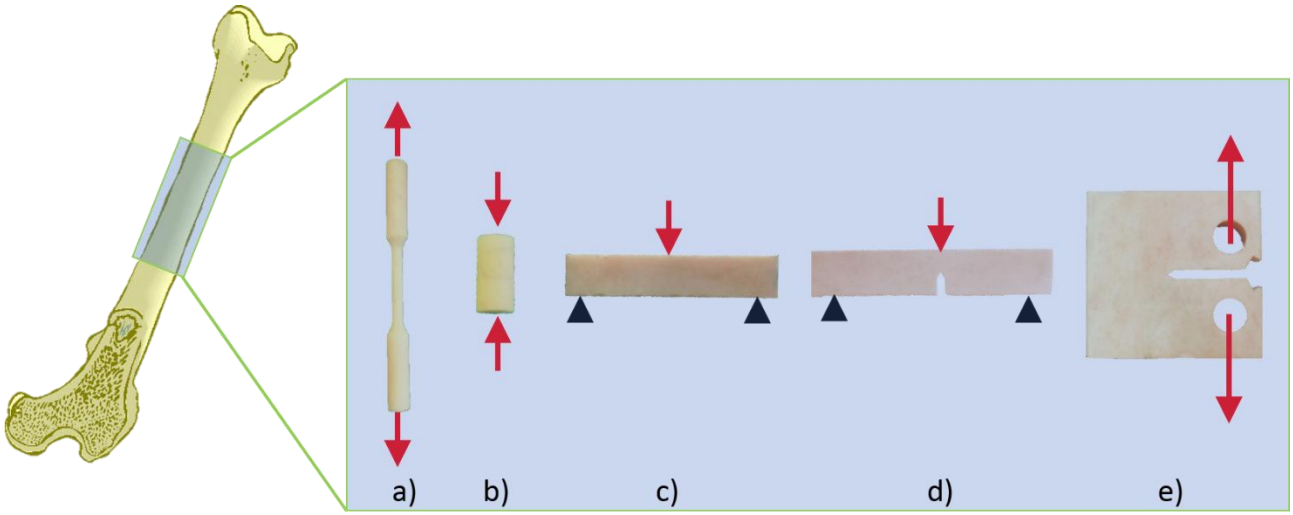

Figure 2 – Schematic view of a bovine femur. Highlighted the area of samples cutting (i.e. diaphysis). Sample geometry for each type of performed test: a) dogbone sample for tensile testing, b) cylindrical sample for compressive t., c) rectangular prismatic sample for three-point bending t., d) SE(B) sample for fracture toughness t., e) C(T) samples for fracture toughness t.

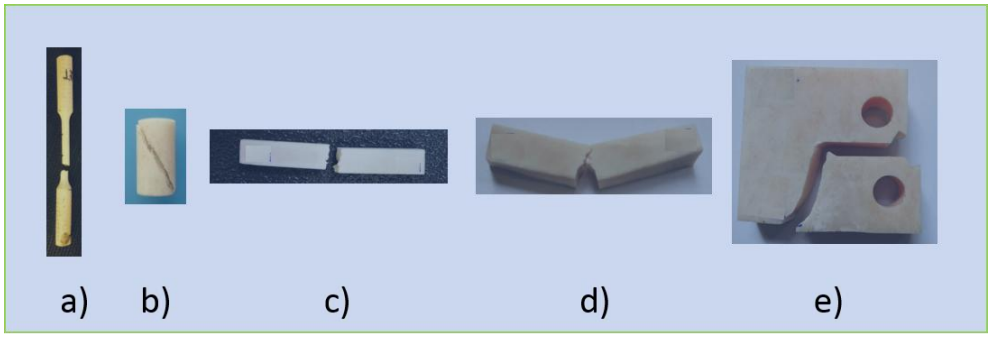

Figure 3 – Failure mode of all the samples: a) Tensile, b) Compressive, c) Flexural, d) SE(B) for fracture toughness, and e) C(T) for fracture toughness.

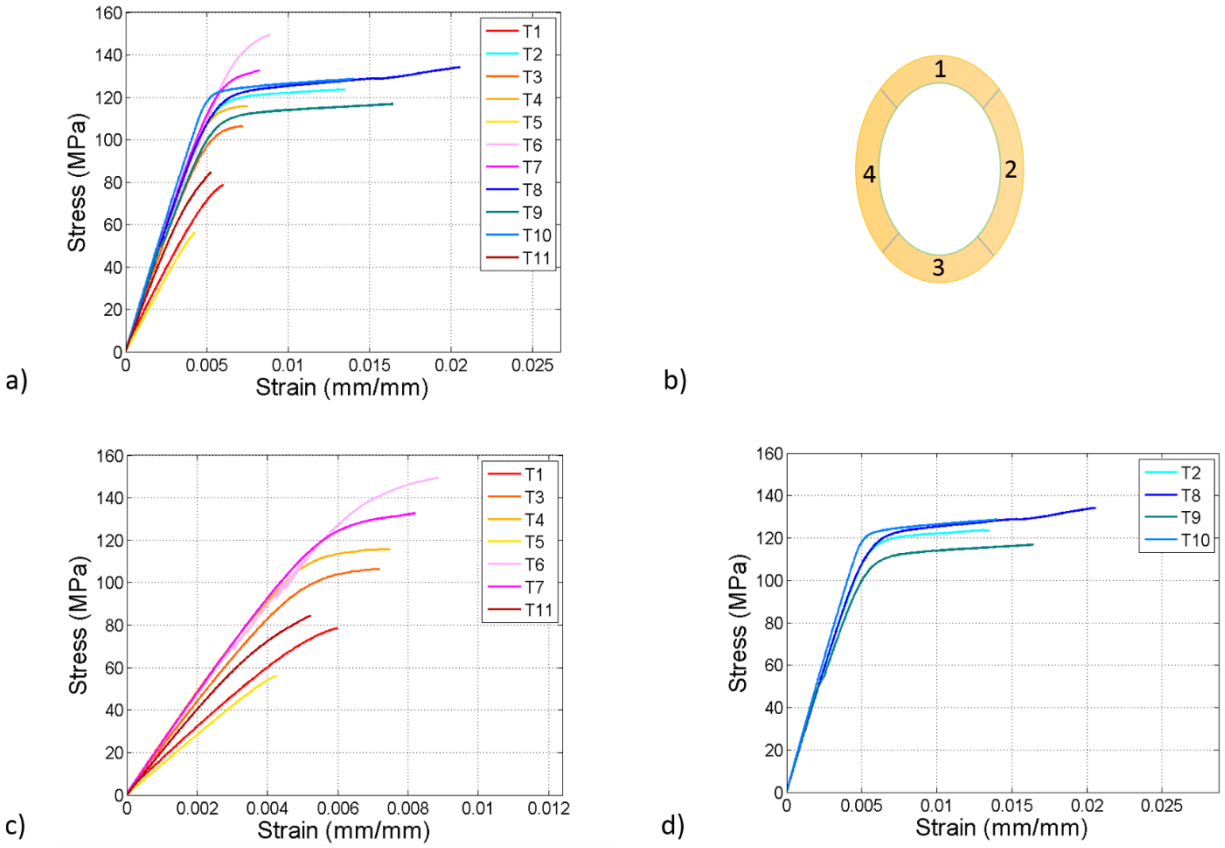

Figure 4 – a) Stress-strain curves resulting from tensile tests. b) Cross section of the diaphysis of the femur: indicated the four regions from which we cut samples: anterior (region 1), posterior (region 3) and lateral (region 2-4). It is possible to distinguish two types of mechanical behaviors: c) linear elastic behavior; d) elastic-plastic behavior. Samples of group c) correspond to the anterior region of the diaphysis (region 1 in panel b), whereas samples of group d) correspond to the lateral-to-posterior regions (region 2-3 in panel b).

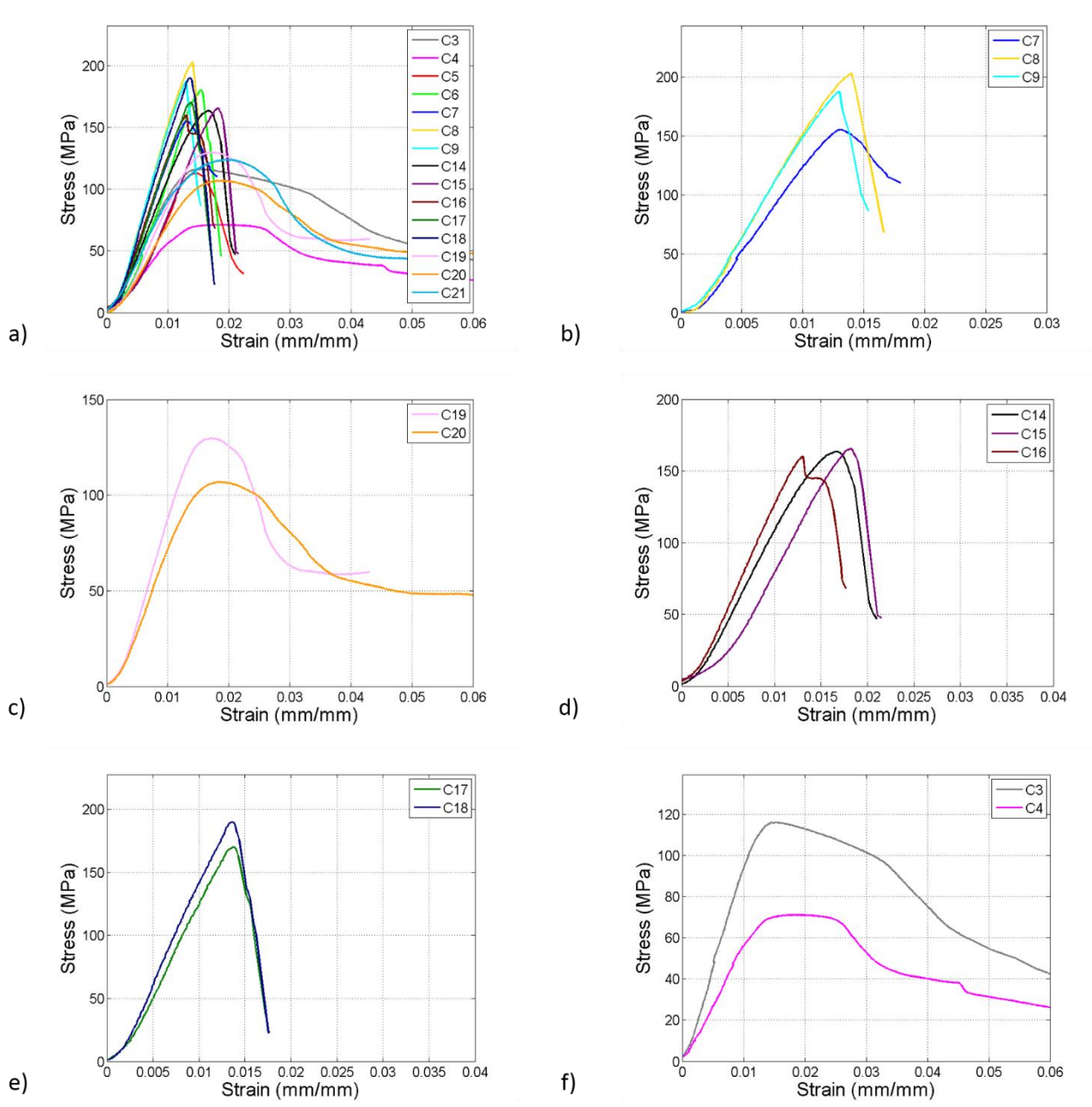

Figure 5 – Stress-strain curves resulting from compressive tests: the stress-strain trends show a high data scattering. Moreover, also in this case there is clear dependence of the mechanical behavior on the anatomical region of the sample. a) Stress-strain curves of all the compression tests carried out at a 0.7 mm crosshead speed. b) Stress-strain curves of compressive behavior of samples taken from the anterior region (*i.e.* region 1 in Figure 4b). c) Stress-strain curves of compressive behavior of samples taken from the posterior region (*i.e.* region 3 in Figure 4b) of distal part of the diaphysis. d) Stress-strain curves of compressive behavior of samples taken from the posterior region (*i.e.* region 3 in Figure 4b) of the proximal part of the diaphysis. e) Stress-strain curves of compressive behavior of samples taken from the lateral region (*i.e.* region 4 in Figure 4b) of distal part of the diaphysis. f) Stress-strain curves of compressive

behavior of samples taken from the lateral region (*i.e.* region 4 in Figure 4b) of the proximal part of the diaphysis.

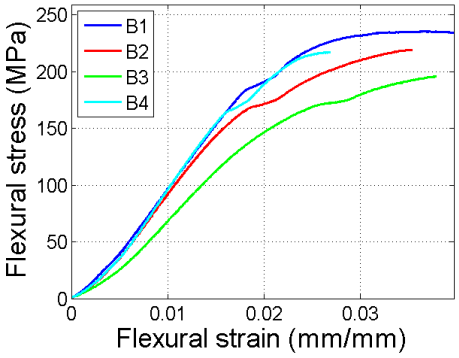

Figure 6 – Stress-strain curves resulting from three-point bending tests. In this case, the samples have a similar trend and the results show a good repeatability in terms of stiffness, strength and strain.

a) 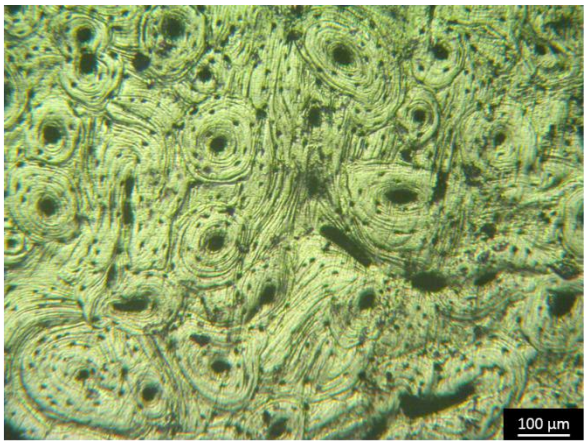

b) 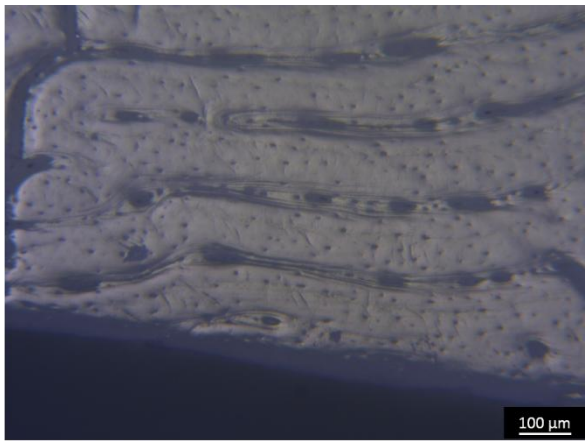

Figure 7 – Images taken with an OM and showing the transversal surfaces of cortical bone tissue from an optical microscope. a) Secondary or Haversian structure. It is possible to recognize the main structural features: *i.e.* the osteons, the lamellae, the Haversian canals, the canaliculi and lacunae. This Haversian structure is very common in the inner zone of the femur cross section (*i.e.* close to the marrow). b) Primary or plexiform structure: the structure is predominantly lamellar, with a limited presence of osteons. This structure is very common near the bone outer cortex. Indeed, in the femur cross section it is possible to note a transition from an osteonal region (*i.e.* inner part, close to the marrow) to a more plexiform region (*i.e.* outer part, close to the outer cortex). In addition, in panel a) and b) it is possible to notice the presence of intrinsic defects, such as porosities, and manufacturing-induced microdamages, such as microcracks.

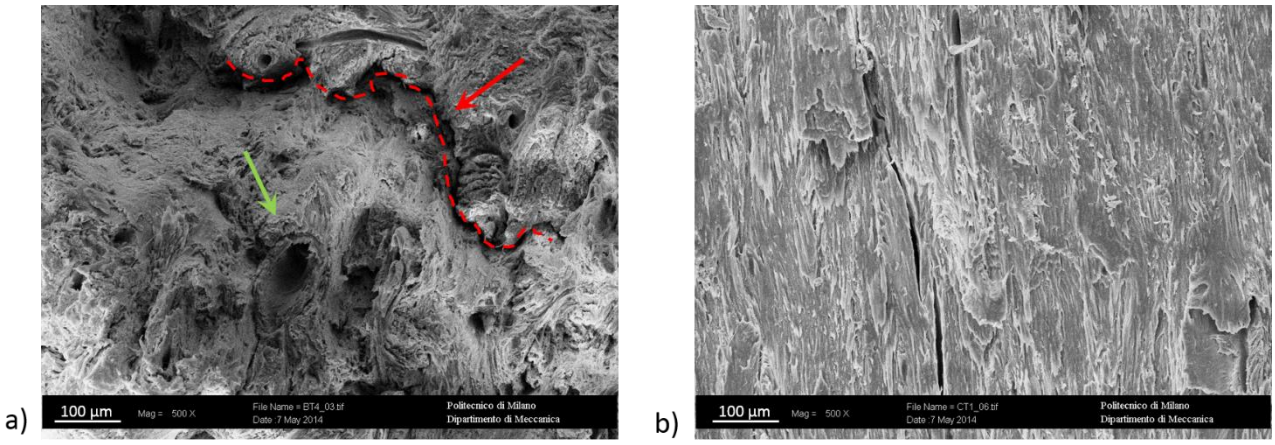

Figure 8 – Micrographies of fracture surfaces of cortical bone tissue from SEM. a) Fracture surface of an SE(B) sample, subjected to a fracture toughness test. The surface is very rough and shows large inelastic deformation. Also, it is possible to recognize the classic toughening mechanisms of osteon pullout (indicated by a green arrow) and crack deflection (indicated by a red arrow and a red dashed line). b) Fracture surface of a C(T) sample, subjected to a fracture toughness test. The surface is less rough than that shown in panel a) and referred to an SE(B) sample. Indeed, in this case the crack showed a 90° deflection and the sample failed by longitudinal splitting.

Table_1

Table 1 - Literature review of the mechanical properties of human and bovine cortical bone tissues, experimentally determined through different techniques.

Authors	Type of bone	E [GPa]	J_c [N/m]	K_c [MPa$\sqrt{m}$]	K_{JIc} [MPa$\sqrt{m}$]	Test method
Rho *et al.* [13]	Cortical (human tibia)	22.5 ± 1.3 (osteon tissue) 25.8 ± 0.7 (interstitial lamellae)	-	-	-	Nanoindentation
Thurner *et al.* [15]	Cortical (human femur)	20.55±0.21 (longitudinal) 23.45±0.21 (longitudinal)	-	-	-	Acoustic measurement Nanoindentation
Rho *et al*. [30]	Cortical (human)	20.7 ± 1.9 * 18.6 ± 3.5 **	-	-	-	*Ultrasonic technique **Microtensile testing
Zysset *et al.* [41]	Cortical (human femur)	20.1±5.4	-	-	-	Nanoindentation
Vashishth *et al.* [51]	Cortical (bovine femur)	-	-	3.9-7.2	-	Fracture toughness tests on C(T) samples
Yan *et al.* [49]	Cortical (bovine femur)	17.5 (transverse-fractured) 12.1 (longitudinal-fractured)	6.6 ± 0.8 2.3 ± 0.3	5.1 ± 0.5 2.6 ± 0.3	10.5 ± 0.5 6.2 ± 0.3	Fracture toughness tests on SE(B) (with grooves)
Koester *et al.* [2]	Cortical (human humerus)	-	-	-	25 (crack length < 500 μm) 5 (crack length 7000 μm)	Fracture toughness tests on SE(B) and C(T) samples
Zimmermann *et al.* [56]	Cortical (human femur)	15.70 ± 3.5 (young) 15.85 ± 3.3 (aged)	-	-	11-14 (stress intensity rate 0.01 MPa$\sqrt{m}\cdot s^{-1}$	Fracture toughness tests on SE(B) samples

Table_2

Table 2 - Experimental results of the mechanical characterization performed on cortical bovine bone samples. For the determination of K_{Jc} we used the value of E', calculated from the Young modulus, E, experimentally determined by means of tensile tests.

	Tensile test	Compression test	Flexural test	Fracture Toughness test SE(B)	Fracture Toughness test C(T)
***E* [GPa]**	19.6 ± 4.5	12.4 ± 3.2	11.5 ± 0.6	-	-
σ_y [MPa]	105.3 ± 26.1	145.5 ± 36.8	-	-	-
σ_U [MPa]	111.3 ± 27.4	149.1 ± 37.2	223.4 ± 9.5	-	-
K_Q [MPa√m] (E399) [60]	-	-	-	4.4 ± 0.8	5.4 ± 0.8
J_{tot} [KJ/m^2] (ASTM E1820) [61]	-	-	-	4.9 ± 1.7	4.4 ± 1.7[1]
K_{Jc} [MPa√m] (ASTM E1820) [61]	-	-	-	10.6 ± 1.7	10.0 ± 1.8[1]

[1]The values of J_c and K_{Jc} are only estimates, since the C(T) samples are designed according to ASTM E399 [60], hence we did not measure the load-line displacement as required by [61].

figure_1.tif
Click here to download high resolution image

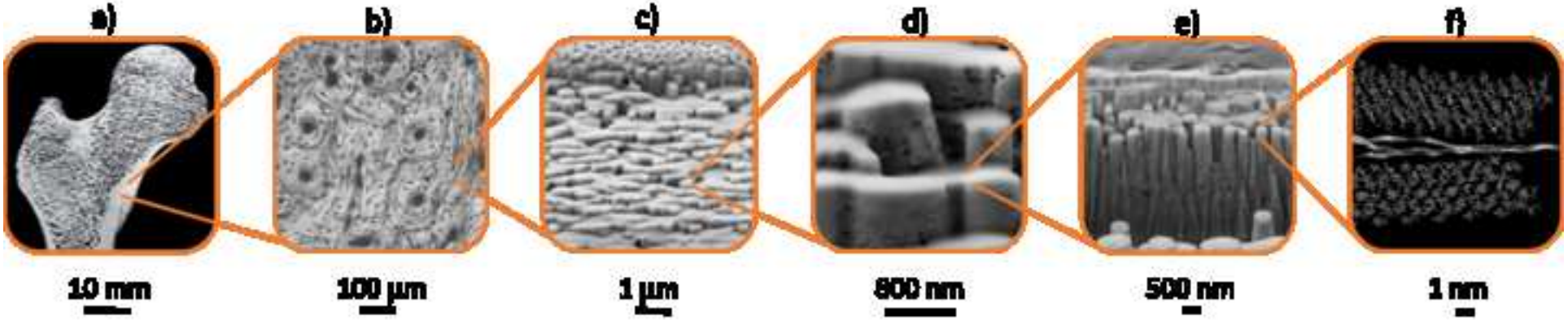

figure_2.tif
Click here to download high resolution image

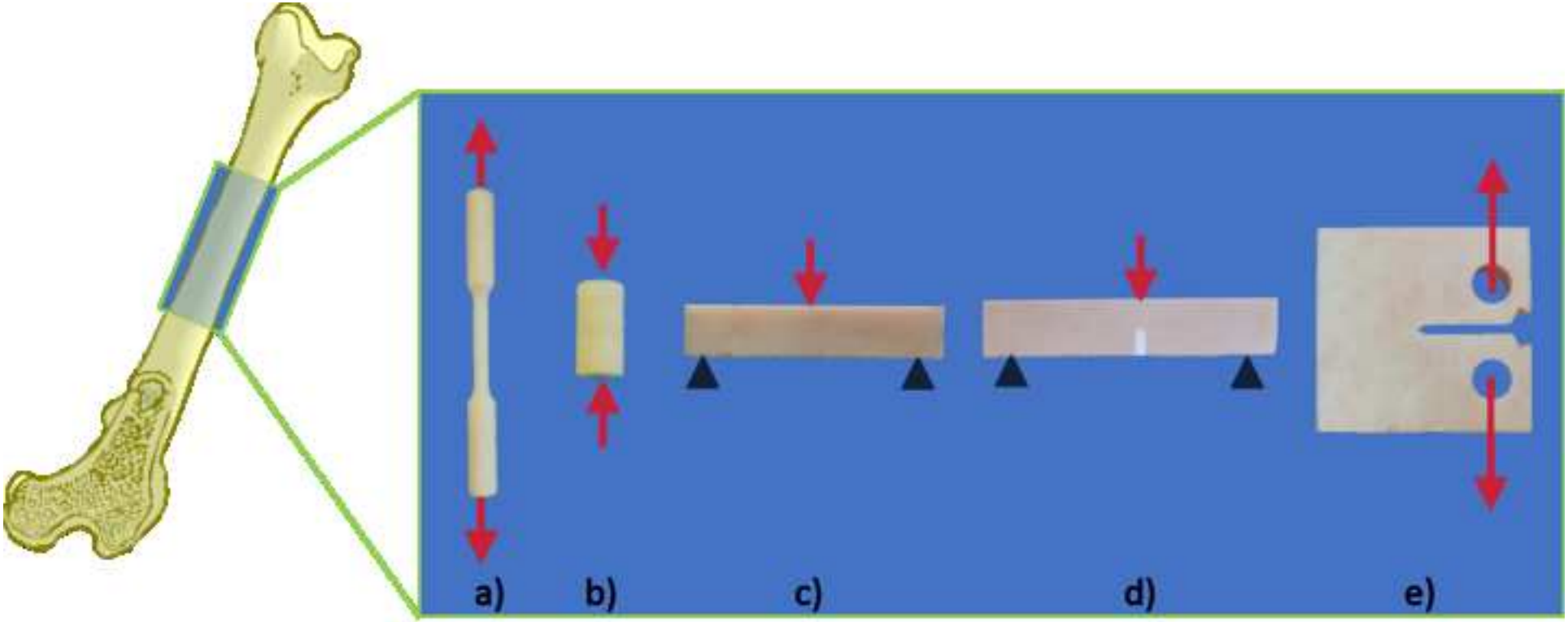

figure_3.tif
Click here to download high resolution image

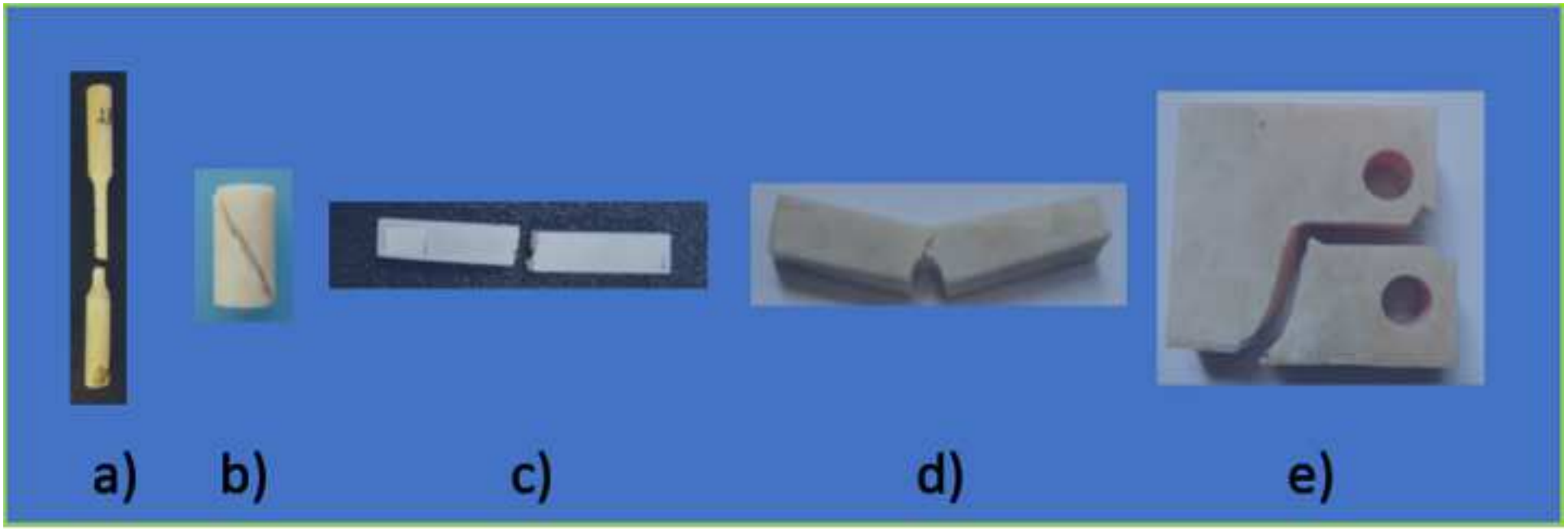

figure_4.tif
Click here to download high resolution image

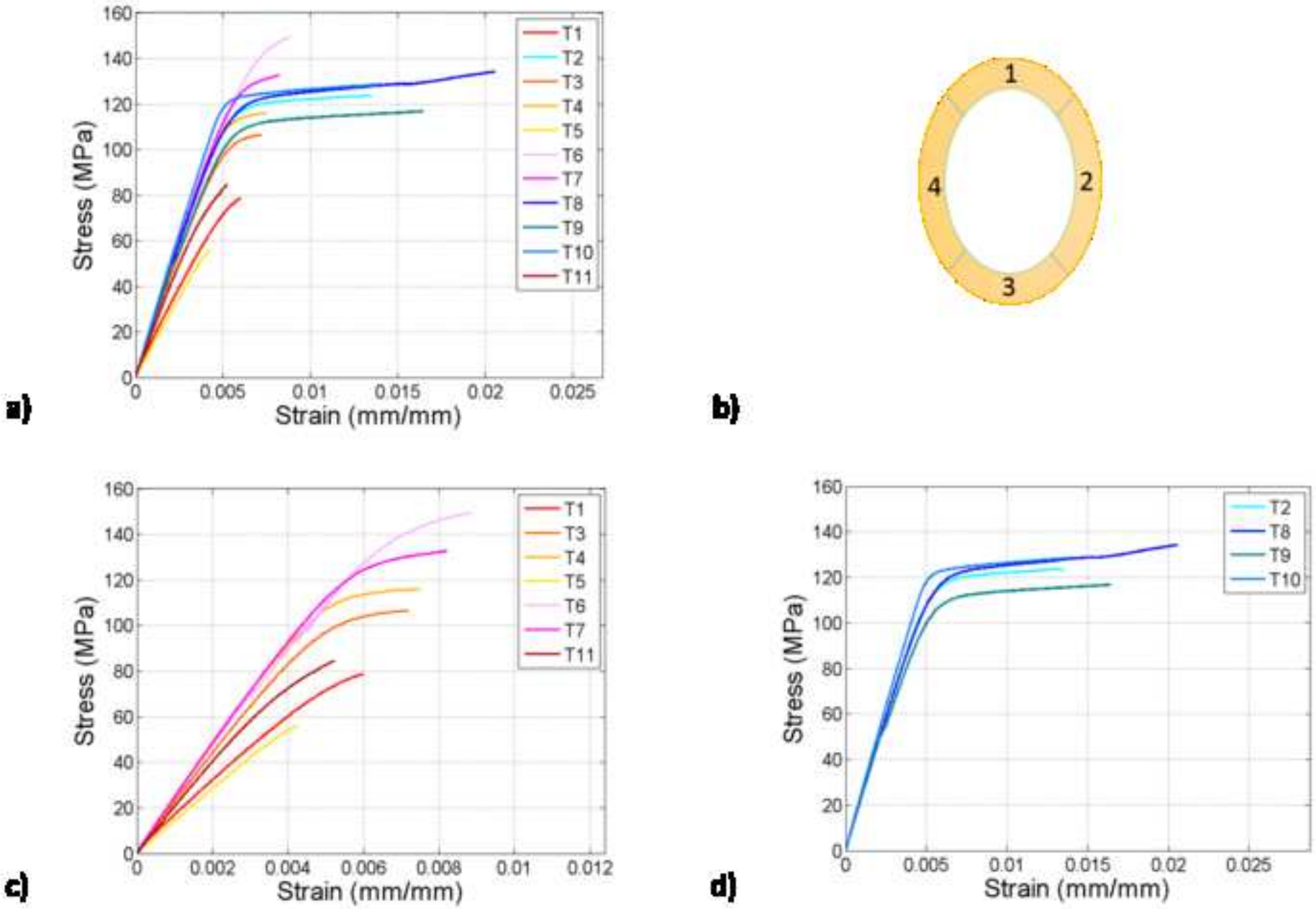

figure_5.tif
Click here to download high resolution image

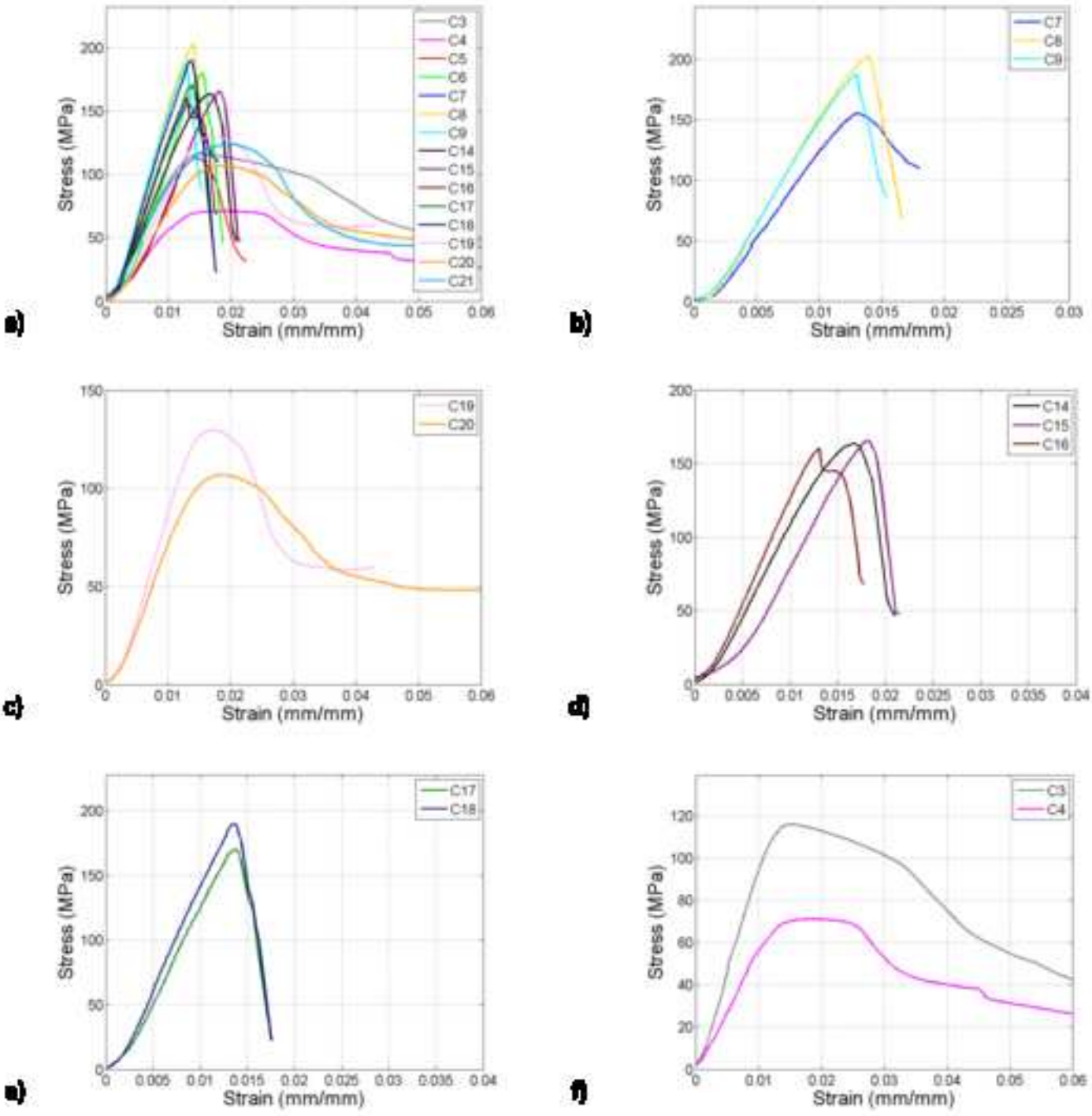

figure_6.tif
Click here to download high resolution image

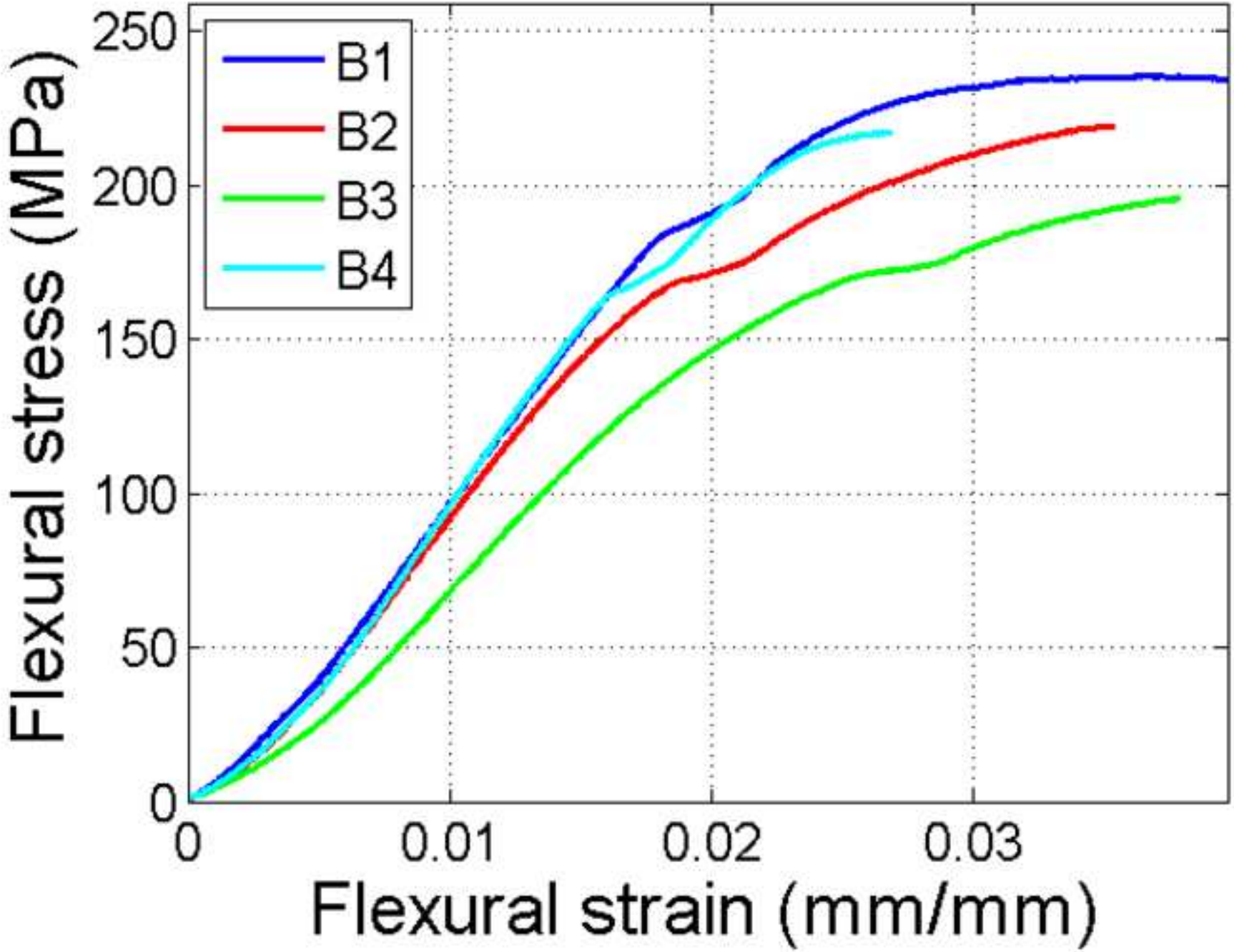

figure_7.tif
Click here to download high resolution image

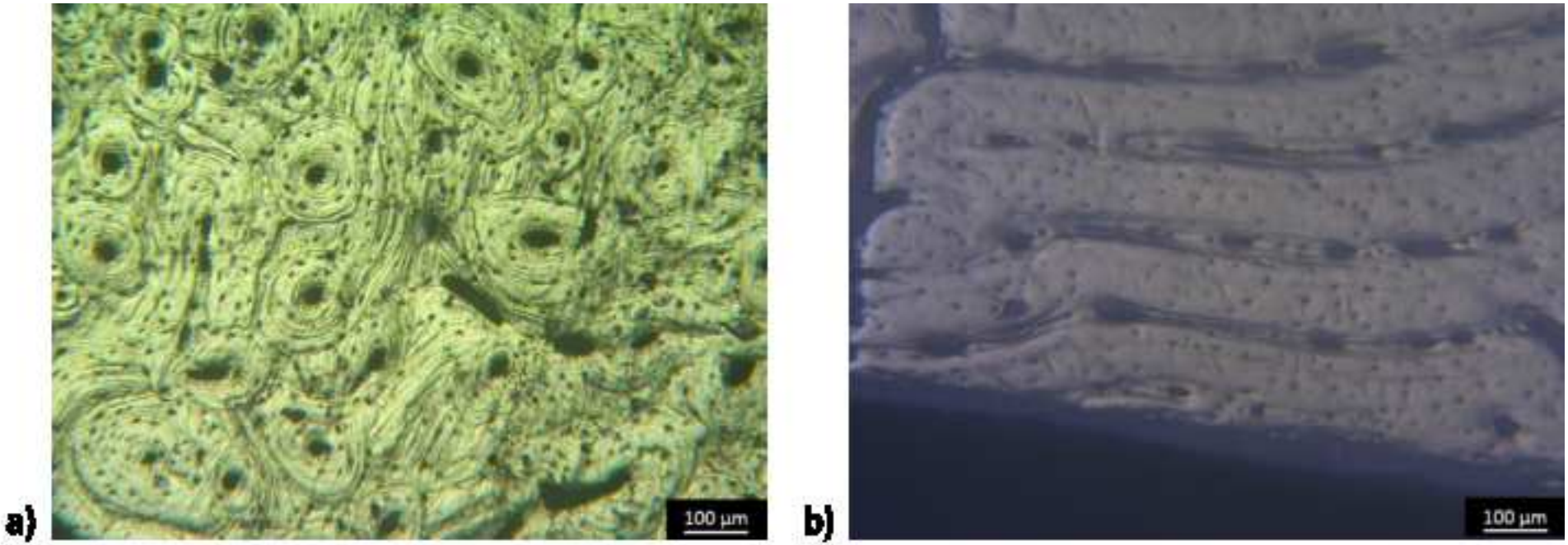

figure_8.tif
Click here to download high resolution image